

χ_{cJ} production associated with a $c\bar{c}$ pair at hadron colliders

Dan Li,¹ Yan-Qing Ma,¹ and Kuang-Ta Chao^{1,2}

¹*Department of Physics and State Key Laboratory of Nuclear Physics and Technology,
Peking University, Beijing 100871, China*

²*Center for High Energy Physics, Peking University, Beijing 100871, China*

(Dated: February 17, 2022)

Abstract

χ_{cJ} ($J=0,1,2$) production associated with a charm quark pair in hadron collisions is calculated in the framework of nonrelativistic QCD at the Tevatron and LHC. It is found that the color-singlet contribution is small and the color-octet contribution may be dominant in the large p_T region. The differential cross section of $p\bar{p} \rightarrow \chi_c + c\bar{c}$ is at least one order of magnitude smaller than the next-to-leading order result of χ_{cJ} inclusive production $p\bar{p} \rightarrow \chi_c + X$, therefore χ_{cJ} production in $p\bar{p} \rightarrow \chi_c + c\bar{c}$ may have negligible influence on the ratio $R_{\chi_c} = \frac{\sigma_{\chi_{c2}}}{\sigma_{\chi_{c1}}}$ measured by CDF at the Tevatron. The feeddown contribution from $\chi_{cJ} + c + \bar{c}$ to $J/\psi + c + \bar{c}$ is found to be large compared with J/ψ direct production and may have important influence on the measurement of $J/\psi + c + \bar{c}$. The validity of fragmentation approximation for the process is also discussed.

PACS numbers: 12.38.Bx, 13.60.Le, 14.40.Pq

I. INTRODUCTION

Charmonium production associated with a $c\bar{c}$ pair is a good experimental observable in understanding the production mechanism of heavy quarkonium. The associated production has been extensively studied in the literature. In e^+e^- annihilation at B factories, $J/\psi + c + \bar{c}$ was found to have a very large fraction of J/ψ inclusive production[1, 2]. This phenomena can be understood by a large next-to-leading order (NLO) QCD correction to the color-singlet (CS) $J/\psi + c + \bar{c}$ production[3], and a relatively small NLO QCD correction to the CS $J/\psi + X_{non-c\bar{c}}$ production[4]. These studies also imply that the color-octet (CO) contribution to J/ψ production may be very small and even negligible, and a set of severe constraint on the linear combination of related CO matrix elements was further obtained by analyzing J/ψ production in e^+e^- annihilation[5]. At LEP, in the Z^0 decay, $J/\psi + c + \bar{c}$ [6] was found to be the dominant contribution to the J/ψ inclusive production[7]. On the contrary, in $\gamma\gamma$ collisions, the contribution of J/ψ associated production [8] was estimated to be several orders of magnitude smaller than the experimental data of J/ψ inclusive production[9]. In hadron collisions at the Tevatron, theoretical predictions[10, 11] showed that the $J/\psi + c + \bar{c}$ contribution was significant in the large p_T region compared with the NLO result of non- $c\bar{c}$ contributions, and the produced J/ψ is mainly unpolarized, which is analogous to the polarization of J/ψ in inclusive production[12, 13]. The integrated cross section was also significant and showed a great measurable potential both at the Tevatron and RHIC. J/ψ associated production was also considered in the Υ decay[14] to explore the CO mechanism in heavy quarkonium decays. As shown, most of those studies focused on J/ψ associated production. However, due to the importance of charmonium associated production, studies of associated production for other charmonium states other than J/ψ may also be valuable.

In this paper, we perform a calculation for the P-wave charmonium χ_{cJ} ($J=0,1,2$) associated production in hadron collisions in the framework of nonrelativistic QCD(NRQCD)[15]. The motivation for this work is two fold. The first is related to the ratio $R_{\chi_c} = \frac{\sigma_{\chi_{c2}}}{\sigma_{\chi_{c1}}}$ measured by the CDF collaboration at the Tevatron. CDF found that R_{χ_c} approaches to about 0.75 at large p_T [16]. However, if the χ_{cJ} inclusive production is dominated by the CO process (because the CS contribution at large p_T is suppressed by $\frac{1}{p_T^2}$ at leading order(LO)), the value of R_{χ_c} should tend to be $\frac{5}{3}$, which is predicted by naive spin counting. Recently, the calculation of NLO QCD correction to $\chi_{cJ} + X_{non-c\bar{c}}$ inclusive production is performed[17]

and it is found that the NLO correction for CS channel can bring out a $\frac{1}{p_T^4}$ term, which makes the CS contribution much important at large p_T , and then by combining CS with CO contributions one is able to fit the experimental value of R_{χ_c} quite well over a wide p_T region. The χ_{cJ} associated production with a $c\bar{c}$ pair is of the same order in pQCD as the NLO $\chi_{cJ} + X$ inclusive production and it contains also fragmentation contributions which scale as $\frac{1}{p_T^4}$. So it is interesting to check whether the $\chi_{cJ}c\bar{c}$ associated production is also very large and whether it can further improve theoretical predictions of ratio R_{χ_c} . The second reason is that the measurements at the Tevatron for the production rates of $J/\psi + c + \bar{c}$ and $J/\psi + X$ are important on shedding light on understanding the J/ψ production mechanism in hadron collisions. And the prompt J/ψ production receives significant feeddown contributions from $\psi(2S)$ and χ_{cJ} . So it is important to know how large is the feeddown contribution to J/ψ associated production from χ_{cJ} associated production. The result itself in this work can also give information for directly measuring χ_{cJ} from $\chi_{cJ} + c + \bar{c}$ production at hadron colliders.

The remainder of this paper is organized as follows. In Sec. II we briefly describe our calculation method. In Sec. III we give our numerical results and analyze the obtained results. In the last section, we give a summary.

II. CALCULATION OF $p\bar{p} \rightarrow \chi_{cJ} + c + \bar{c}$

In the framework of NRQCD factorization, the cross section for the $\chi_{cJ}c\bar{c}$ associated production in proton-antiproton collisions has the following form:

$$d\sigma[p\bar{p} \rightarrow \chi_{cJ} + c + \bar{c}] = \sum_{i,j,n} \int dx_1 dx_2 f_{i/p}(x_1) f_{j/\bar{p}}(x_2) \times d\hat{\sigma}(i + j \rightarrow c\bar{c}[n] + c + \bar{c}) \langle O^{\chi_{cJ}}[n] \rangle \quad (1)$$

where i, j denote the initial state partons from the proton or anti-proton. We assume the contribution from light quark annihilation to be negligible, so i, j are gluons in our case. The quantum numbers n represent the color and orbital angular momentum of the intermediate $c\bar{c}$ states at short-distances, which evolve into the χ_{cJ} meson at long-distances. At leading order in relative velocity v of the $c\bar{c}$ pair, n can be taken as $n = {}^3P_J^{[1]}$ for the CS and $n = {}^3S_1^{[8]}$ for the CO intermediate states. We use **FeynArts**[18] to generate Feynman diagrams. For the CS case, there are 56 Feynman diagrams, of which some representative are shown in Fig.

1. For the CO case, there are 16 extra Feynman diagrams relative to the CS case and their extra topology structures are shown in Fig. 2. These extra topology structures actually represent gluon fragmentation contributions.

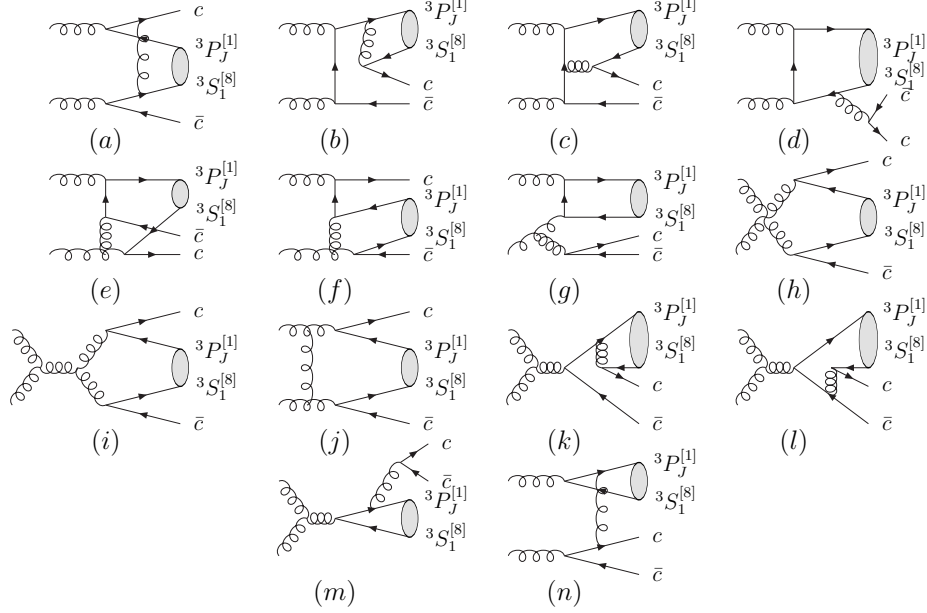


FIG. 1: Representative Feynman diagrams for $p\bar{p} \rightarrow \chi_{cJ} + c + \bar{c}$.

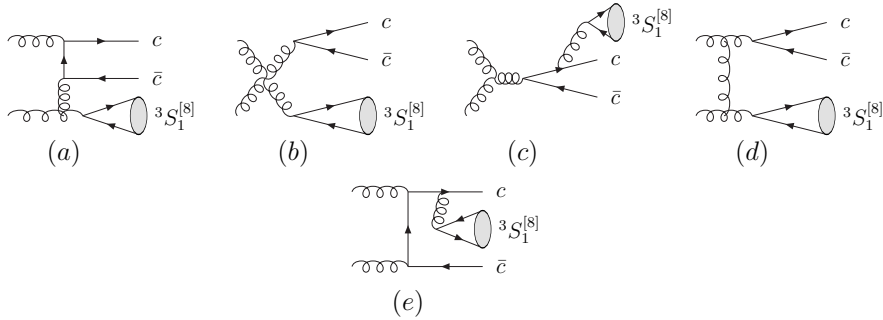


FIG. 2: Representative extra diagrams for CO channel.

The fragmentation diagrams can give a $\frac{1}{p_T^4}$ contribution for the differential cross section $\frac{d\sigma}{dy dp_T^2}$, while remained diagrams can at most give $\frac{1}{p_T^6}$ terms. Therefore, one may expect the fragmentation contribution is dominant at large p_T . Note that, however, not only the CO channel ($^3S_1^{[8]}$) have fragmentation contribution, but the CS channel has also quark (anti-quark) fragmentation contributions. In Fig.1, the diagrams (b) and (k) represent (anti-

)quark fragmentation contributions in the large p_T approximation, where one of the charm or anti-charm quark fragments to χ_c plus another charm or anti-charm quark. However, only when p_T is large enough, these quark diagrams can reach the fragmentation region and give leading contributions. Otherwise, these quark diagrams can give only small contributions. We will discuss the fragmentation approximation in the next section.

We use the spinor-helicity method to deal with Feynman amplitudes[19] and use the package **S@M**[20] to simplify the Feynman amplitudes in spinor form. Based on this method, the spinor form for massive external fermions can be written as

$$u_{\pm\frac{1}{2}}(p) = \frac{1}{\sqrt{2p \cdot q}}(\not{p} + m)|q_{0\pm}\rangle, \quad (2)$$

$$v_{\pm\frac{1}{2}}(p) = \frac{1}{\sqrt{2p \cdot q}}(\not{p} - m)|q_{0\mp}\rangle, \quad (3)$$

where $u_{\pm\frac{1}{2}}(p)(v_{\pm\frac{1}{2}}(p))$ are Dirac spinors of massive (anti-)fermion with momentum p and spin $\pm\frac{1}{2}$; $q_{0\pm}$ are reference Weyl spinors with light-like reference momentum q_0 and helicities $\lambda = \pm 1$. In principle, \vec{q}_0 should be along the axis of \vec{p} to guarantee the validity of above equations for individual spin. However, if we just concern about a result by summing over spin, q_0 can be chosen arbitrarily. Here, it is chosen to be one of the initial partons' momentum in order to simplify the calculation. The polarization vectors for external gluon with momentum k and light-like reference momentum q_0 are represented as

$$\epsilon^+(k, q_0) = \frac{\sqrt{2}}{\langle q_0 | k \rangle}(|k_-\rangle\langle q_{0-}| + |q_{0+}\rangle\langle k_+|), \quad (4)$$

$$\epsilon^-(k, q_0) = \frac{\sqrt{2}}{\langle q_0 | k \rangle^*}(|k_+\rangle\langle q_{0+}| + |q_{0-}\rangle\langle k_-|). \quad (5)$$

Using the following identity, we decouple the spin projection operator[21] for bound states from Feynman amplitudes:

$$\sum_{\lambda_2 \lambda_3} (\not{p}_{\bar{c}} - m_c)|q_{0\lambda_2}\rangle\langle q_{0\lambda_2}|P_{1S_z}|q_{0\lambda_3}\rangle\langle q_{0\lambda_3}|(\not{p}_c - m_c) = 2p_c \cdot q_0 2p_{\bar{c}} \cdot q_0 P_{1S_z}, \quad (6)$$

where there is a relative velocity v between p_c and $p_{\bar{c}}$ for the P-wave case. Then with the help of Fierz transformation (and its generalized forms), the amplitudes are reduced to

$$M_i = C_i^{jk} f_j f_k, \quad (7)$$

where i is the index for different diagrams and f_j are the simplified fermion chains, and the three-gluon vertex are properly dealt with (see [19] for details). The specific expressions of f_j encountered here are listed in the appendix.

We write the polarization tensors for χ_{cJ} explicitly. For χ_{c0} it is symmetric for the two indexes $\mu\nu$:

$$\epsilon^{\mu\nu} = -g_{\mu\nu} + \frac{p_\mu p_\nu}{m_c^2}; \quad (8)$$

for χ_{c1} it is anti-symmetric for the two indexes $\mu\nu$:

$$\epsilon_1^{\mu\nu} = \frac{1}{\sqrt{2}}(\epsilon_x^\mu \epsilon_y^\nu - \epsilon_x^\nu \epsilon_y^\mu), \quad (9)$$

$$\epsilon_2^{\mu\nu} = \frac{1}{\sqrt{2}}(\epsilon_x^\mu \epsilon_z^\nu - \epsilon_x^\nu \epsilon_z^\mu), \quad (10)$$

$$\epsilon_3^{\mu\nu} = \frac{1}{\sqrt{2}}(\epsilon_y^\mu \epsilon_z^\nu - \epsilon_y^\nu \epsilon_z^\mu); \quad (11)$$

for χ_{c2} it is again symmetric for the two indexes $\mu\nu$:

$$\epsilon_1^{\mu\nu} = \frac{1}{\sqrt{2}}(\epsilon_x^\mu \epsilon_y^\nu + \epsilon_x^\nu \epsilon_y^\mu), \quad (12)$$

$$\epsilon_2^{\mu\nu} = \frac{1}{\sqrt{2}}(\epsilon_x^\mu \epsilon_z^\nu + \epsilon_x^\nu \epsilon_z^\mu), \quad (13)$$

$$\epsilon_3^{\mu\nu} = \frac{1}{\sqrt{2}}(\epsilon_y^\mu \epsilon_z^\nu + \epsilon_y^\nu \epsilon_z^\mu), \quad (14)$$

$$\epsilon_4^{\mu\nu} = \frac{1}{\sqrt{2}}(\epsilon_x^\mu \epsilon_x^\nu - \epsilon_y^\nu \epsilon_y^\mu), \quad (15)$$

$$\epsilon_5^{\mu\nu} = \frac{1}{\sqrt{6}}(\epsilon_x^\mu \epsilon_x^\nu + \epsilon_y^\mu \epsilon_y^\nu - 2\epsilon_z^\mu \epsilon_z^\nu). \quad (16)$$

The definition of ϵ_x , ϵ_y , and ϵ_z are

$$\epsilon_x(P) = (0, \cos \theta \cos \phi, \cos \theta \sin \phi, -\sin \theta), \quad (17)$$

$$\epsilon_y(P) = (0, -\sin \phi, \cos \phi, 0), \quad (18)$$

$$\epsilon_z(P) = \frac{1}{M}(|\vec{P}|, P_0 \sin \theta \cos \phi, P_0 \sin \theta \sin \phi, P_0 \cos \theta), \quad (19)$$

where M , \vec{P} , and P^0 are the mass, momentum and energy of χ_{cJ} ; angles θ and ϕ describe χ_{cJ} 's direction[22]. For CO $^3S_1^{[8]}$, the spinor-helicity forms of polarization vectors are kept as $\langle q_{0\lambda} | \not{\epsilon} | q_{0\lambda} \rangle$, $\langle q_{0\lambda} | \not{\epsilon} \not{p} | q_{0\lambda} \rangle$, $\langle q_{0\lambda} | \not{p} \not{\epsilon} | q_{0\lambda} \rangle$ until numerically squaring the amplitudes in Fortran program.

In our numerical calculation, we give only a rapidity cut condition for χ_c . However, to detect the associated production, one should detect at least another hadron containing charm or anti-charm quark, and the rapidity cuts from experimental facility should also apply for the (anti-)charm quarks in principle.

For phase space integration, we use the general $2 \rightarrow 3$ phase space expression, plus two fold momentum fraction integration for initial partons:

$$\frac{d\sigma}{dp_T} = \int_{\delta}^1 dx_1 f_{g/p}(x_1) \int_{\delta/x_1}^1 dx_2 f_{g/\bar{p}}(x_2) \int_{\sqrt{m_5^2 + p_T^2}}^{(k_5^0)_{max}} dk_5^0 \int_{(k_3^0)_{min}}^{(k_3^0)_{max}} dk_3^0 \int_0^{2\pi} d\eta \sum |M|^2, \quad (20)$$

where $\delta = \frac{16m^2 + 4p_T^2}{s}$, k_5^0 is the energy of χ_c , k_3^0 is the energy of one of the emitted charm or anti-charm quark, η describes the angle between the plane for the final three particles and the plane chosen for the two initial partons, and we omit flux factor and other normalization factors. The upper and low limits for k_5^0 and k_3^0 integration are a little complicated so we don't list them here. We use Vegas [23] in Fortran program to perform the numerical integration. The correctness of our phase space integration program is verified by comparing the calculated $J/\psi + c + \bar{c}$ production (we calculate it again) with the result from Ref.[10].

III. RESULT AND ANALYSIS

In numerical calculation, we choose $m_c = 1.5\text{GeV}$. The factorization scale and renormalization scale are both chosen as $\mu_0 = \sqrt{p_T^2 + 4m_c^2}$. We use CTEQ6M as PDF input. The CS matrix element $\langle O^{\chi_{cJ}}[{}^3P_J^{[1]}] \rangle$ is related to the P-wave function at the origin by the formula: $\langle O^{\chi_{cJ}}[{}^3P_J^{[1]}] \rangle = \frac{(2J+1)3N_c}{2\pi} |R'_P(0)|^2$ and we choose: $|R'_P(0)|^2 = 0.075\text{GeV}^5$ from the potential model calculations[24]. For the CO matrix element $\langle O^{\chi_{cJ}}[{}^3S_1^{[8]}] \rangle$, by spin symmetry, we have the following relation that $\langle O^{\chi_{c0}}[{}^3S_1^{[8]}] \rangle : \langle O^{\chi_{c1}}[{}^3S_1^{[8]}] \rangle : \langle O^{\chi_{c2}}[{}^3S_1^{[8]}] \rangle = 1 : 3 : 5$ and we use $\langle O^{\chi_{c0}}[{}^3S_1^{[8]}] \rangle \approx 2.2 \times 10^{-3}\text{GeV}^3$ as the central value obtained from fitting the χ_{cJ} inclusive production $p\bar{p}$ to $\chi_{cJ} + X_{non-c\bar{c}}$ at the Tevatron[17].

In Fig. 3, we show both CS and CO contributions to the differential cross section of $\chi_c + c + \bar{c}$. It is found that the CO contribution dominates over production in the large p_T region, and it decreases much slower than that of CS as p_T increases. This seems to conflict with that both of the two channels should behave as $\frac{1}{p_T^4}$ at large p_T . To see this point more clearly, we fit the parton differential cross section (taking out the influence of PDF) with $\frac{1}{p_T^n}$, and it turns out that the CS channel scales roughly as $\frac{1}{p_T^6}$ while the CO channel scales as $\frac{1}{p_T^4}$ in the region $p_T < 17\text{ GeV}$. This implies that the CO contribution in Fig. 2 is dominated by gluon fragmentation just as expected, but the CS channel has not reached the (anti-)quark fragmentation region, and its contribution is still suppressed in the moderately large p_T region (e.g., $p_T \leq 17\text{ GeV}$).

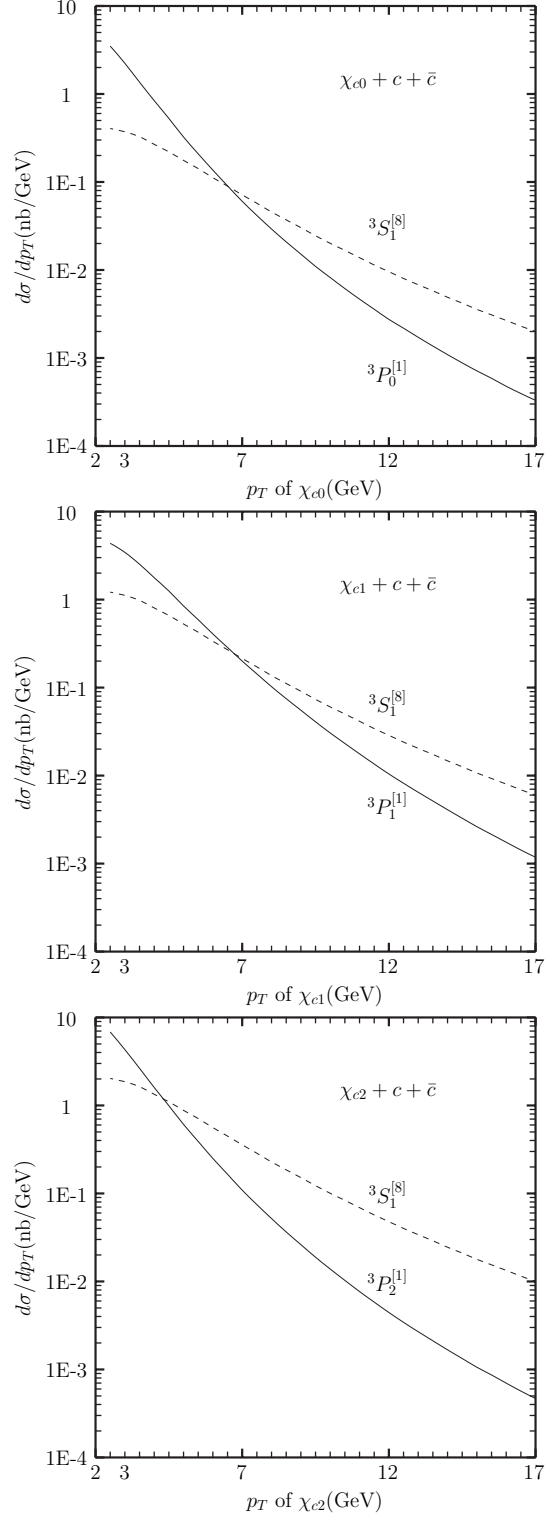


FIG. 3: Differential cross sections of $\chi_{cJ} + c + \bar{c}$ as functions of transverse momentum at the Tevatron with $\sqrt{s} = 1.96$ GeV and rapidity cut $|y_{\chi_{cJ}}| < 0.6$. The dashed line denotes CO contribution, and the solid line denotes CS contribution.

In order to understand the above mentioned p_T behavior, we study the $J/\psi + c\bar{c}$ production as an example. We calculate (anti-)quark fragmentation diagrams in axial gauge to include all $\frac{1}{p_T^4}$ contributions. \sqrt{s} can be set to be 100TeV to enable us to calculate at p_T as large as possible. We find that when $p_T = 50\text{GeV}$, (anti-)quark fragmentation contribution has a fraction of about 70% of the total differential cross section, and then the fraction rises to about 93% when $p_T = 150\text{GeV}$. And the fraction reaches 100% (within the calculation errors) when $p_T > 450\text{GeV}$. Thus we find that (anti-)quark fragmentation approximation is only valid for very large p_T ($p_T > 100\text{GeV}$ at least), while for the presently interested p_T region ($p_T \lesssim 17\text{GeV}$) the $\frac{1}{p_T^4}$ term induced by (anti-)quark fragmentation is very small and not important. This explains the fact that the CS channels in χ_{cJ} production behave almost as $\frac{1}{p_T^6}$.

In Fig. 4, we depict the differential cross section for $\chi_c + c + \bar{c}$ and the NLO result for $\chi_c + X_{non-c\bar{c}}$ [17] as comparison. We find that the contribution from $\chi_c + c + \bar{c}$ is about two orders of magnitude smaller than $\chi_c + X_{non-c\bar{c}}$ at small p_T . The fraction of $\chi_c + c + \bar{c}$ in total $\chi_c + X$ increases gradually and reaches at most 20% at p_T as large as 60GeV. The smallness of the $p\bar{p} \rightarrow \chi_c + c + \bar{c}$ fraction lies in the fact that one of the main sources of $\chi_c + X_{non-c\bar{c}}$ is the CO, which scales as $\frac{1}{p_T^4}$ and begins its contribution at order α_s^3 , while the dominant contribution of $\chi_c + c + \bar{c}$ is suppressed by both α_s and phase space. Based on this analysis, we may conclude that $\chi_c + c + \bar{c}$ has negligible influence on the χ_c inclusive production. As a result, fitting the ratio R_{χ_c} measured by CDF[16] can not be improved by including $p\bar{p} \rightarrow \chi_c + c + \bar{c}$ as compared to the $p\bar{p} \rightarrow \chi_c + X_{non-c\bar{c}}$ result[17].

In the NLO prediction[17], the feeddown contribution of $\chi_{cJ} + X_{non-c\bar{c}}$ possesses about 30% of the prompt J/ψ production rates at $p_T = 20\text{GeV}$ at the Tevatron, and it can give a great influence on J/ψ prompt production. Thus we also evaluate the feeddown contribution of χ_{cJ} to $J/\psi + c + \bar{c}$ to see whether this contribution is also large. In the calculation, we ignore the difference between p_T of J/ψ and χ_c . Note that the feeddown from χ_{cJ} may have important influence on prompt J/ψ 's polarization. This effect relies on χ_{cJ} 's polarized production rates and also the helicity amplitudes of χ_c radiative decays to polarized J/ψ . The related formula can be found in Ref.[25]. In this work, we only consider the unpolarized $\chi_c + c\bar{c}$ production but ignore the polarization effects. The branching ratios for χ_{cJ} radiative decays to J/ψ are $Br(\chi_{c0} \rightarrow J/\psi + \gamma) \approx 0.013$, $Br(\chi_{c1} \rightarrow J/\psi + \gamma) \approx 0.36$, $Br(\chi_{c2} \rightarrow J/\psi + \gamma) \approx 0.20$ respectively[26]. In Fig. 5, we give the feeddown contribution

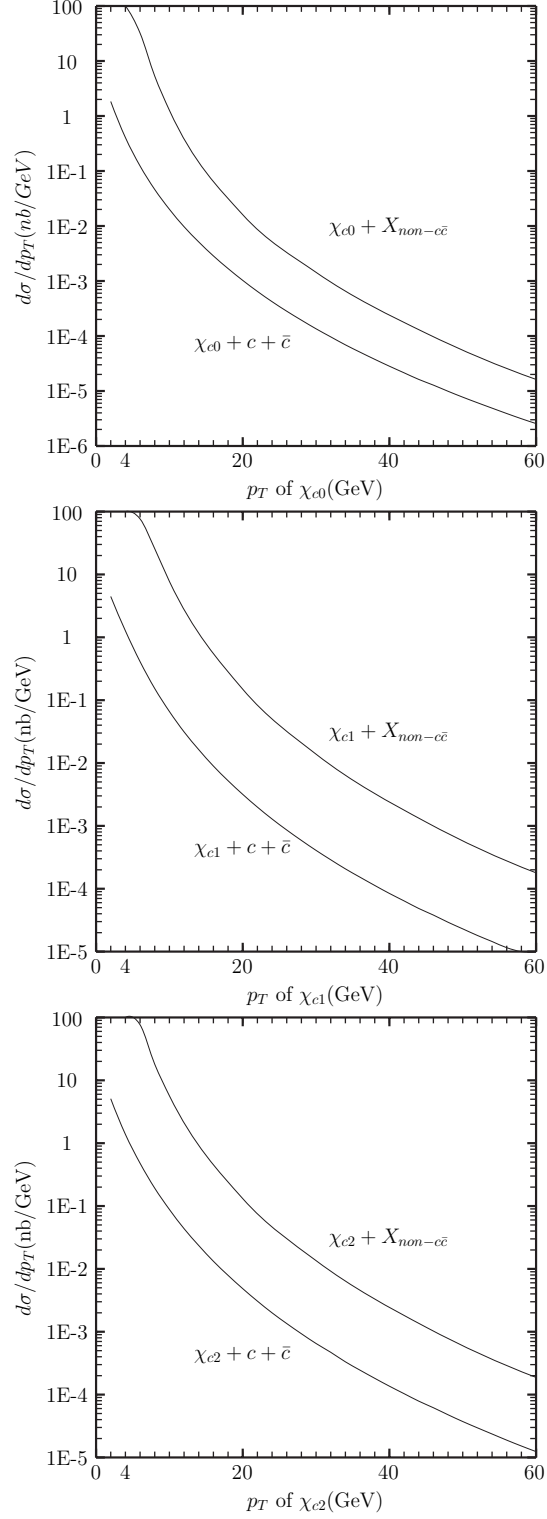


FIG. 4: Comparison of the differential cross sections of $\chi_{cJ} + c + \bar{c}$ with the NLO results of $\chi_{cJ} + X_{non-c\bar{c}}$ at the Tevatron with $\sqrt{s} = 1.96\text{GeV}$ and rapidity cut $|y_{\chi_c}| < 1$.

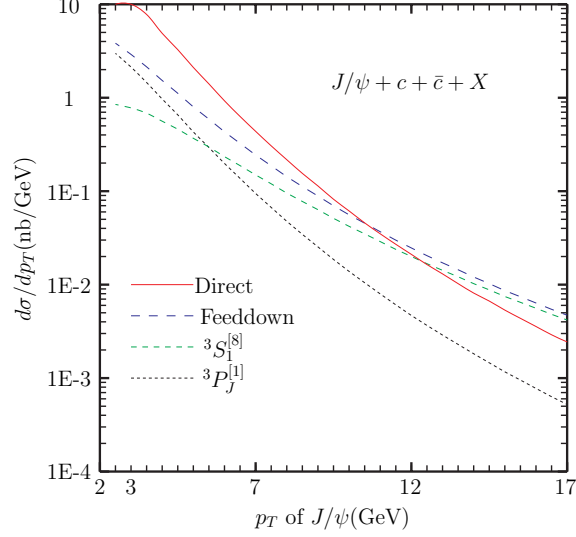


FIG. 5: Contribution of χ_{cJ} feeddown to prompt $J/\psi + c + \bar{c} + X$ production at the Tevatron with rapidity cut $|y_{\chi_c}| < 0.6$. The dotted line denotes the contribution from CS χ_{cJ} feeddown, the short dashed line denotes that from CO χ_{cJ} feeddown, the long dashed line denotes that from CO+CS χ_{cJ} feeddown, and the solid line is the direct $J/\psi + c + \bar{c}$ contribution (from [10]).

from χ_{cJ} as a function of p_T . By comparing it with the direct production, we can see that the feeddown contribution from χ_{cJ} is small in the low p_T region, but it is about a factor of 2 greater than direct $J/\psi + c + \bar{c}$ contribution when $p_T > 15\text{GeV}$. The turning point is at $p_T \approx 9\text{GeV}$ where the feeddown contribution begins to exceed the direct contribution. For $\chi_c + c + \bar{c}$ is dominated by the $^3S_1^{[8]}$ channel at large p_T , one may anticipate that the CO $J/\psi + c + \bar{c}$ contribution from $^3S_1^{[8]}$ may also play an important role in the direct $J/\psi + c + \bar{c}$ production. However, the magnitude depends on the size of $\langle O^{J/\psi}(^3S_1^{[8]}) \rangle$. In a recent work[27], the authors find $\langle O^{J/\psi}(^3S_1^{[8]}) \rangle$ might be small. As a result, χ_c feeddown could become the main source for prompt production of $J/\psi + c + \bar{c}$, if $\langle O^{J/\psi}(^3S_1^{[8]}) \rangle$ is small. Thus when measuring the production cross sections for prompt $J/\psi + c + \bar{c}$ at hadron colliders, the feeddown effect from $\chi_c + c + \bar{c}$ can be very important and should be taken into consideration. We also note that this situation is different from that at B factories, where the $\chi_{cJ} + c + \bar{c}$ production rates in e^+e^- annihilation for both CS and CO are very small, and their feeddown contributions to J/ψ are negligible, therefore, the NLO $J/\psi + c + \bar{c}$ theoretical results (including direct and $\psi(2S)$ feeddown contributions) are basically consistent with experimental production rates. At hadron colliders, however, the $\chi_{cJ} + c + \bar{c}$ feeddown effect

becomes more important.

We also give the prediction of $\chi_{cJ} + c + \bar{c}$ associated production at the LHC with $\sqrt{s} = 7\text{TeV}$. For the CMS detector, the rapidity cut is $|y_{\chi_{cJ}}| < 2.4$ and for the LHCb detector, the rapidity cut is chosen as $2 < y_{\chi_{cJ}} < 4.5$. The results are shown in Fig. 6 and Fig. 7 including the CO contribution, CS contribution and the total differential cross sections. We find that the differential cross sections for $\chi_{cJ} + c + \bar{c}$ associated production at the LHC show a similar behavior as that at the Tevatron: the CO contribution is much larger than CS contribution in almost all p_T region. So χ_{cJ} associated production cross section is dominated by the CO contribution. As a result, measuring $\chi_{cJ} + c + \bar{c}$ production can be used to determine the CO matrix element $\langle O^{\chi_{c0}}[{}^3S_1^{[8]}] \rangle$. Predictions for LHC with $\sqrt{s} = 14\text{TeV}$ and $|y_{\chi_{cJ}}| < 3$ are shown in Fig. 8.

Summary

In this paper, we investigate the χ_{cJ} associated production with a charm quark pair $p\bar{p} \rightarrow \chi_{cJ} + c + \bar{c}$ at hadron colliders in the framework of NRQCD. By comparing the differential cross sections i.e. the transverse momentum distributions for χ_{cJ} associated production, we find that CO dominates the production rate at large p_T . Also, the differential cross sections for associated χ_{cJ} production are at least one order of magnitude smaller than the NLO result for $\chi_{cJ} + X_{non-c\bar{c}}$. As a result, $\chi_{cJ} + c + \bar{c}$ production has negligible influence on the R_{χ_c} value measured by the CDF collaboration. We also evaluate the χ_{cJ} feeddown contribution to prompt $J/\psi + c + \bar{c}$ production, and find that the feeddown contribution is very large compared to direct $J/\psi + c + \bar{c}$ production[10] at large p_T , which illustrates the importance of χ_c feeddown effect in the measurement for J/ψ associated production cross sections and polarization parameters. The fragmentation approximation is analyzed and our conclusion is that the fragmentation contribution is dominant for the CO channel, while for the CS channel the fragmentation diagrams' contribution dominates over the total differential cross section only at the $p_T \gtrsim 100\text{GeV}$ region.

Finally, we note that in the χ_{cJ} associated production, the LO result in α_s has already contained the $1/p_T^4$ term, which is the leading term in $1/p_T$ expansion at large p_T , and high order corrections in α_s can at most give the $1/p_T^4$ term, but suffer from suppressions due to extra powers of α_s . So we expect that high order corrections in α_s can not significantly

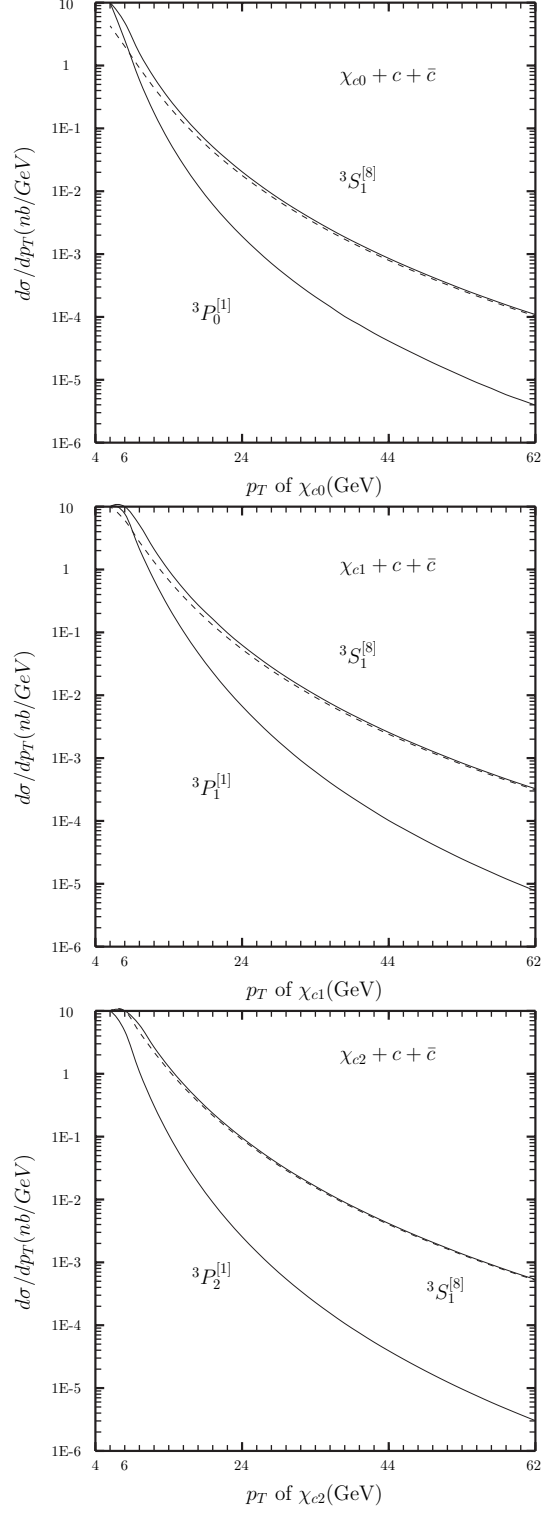


FIG. 6: Differential cross sections of $\chi_{cJ} + c + \bar{c}$ as functions of transverse momentum at the LHC with $\sqrt{s} = 7$ TeV and rapidity cut $|y_{\chi_{cJ}}| < 2.4$. The dashed line denotes CO contribution, and the solid line denotes CS contribution.

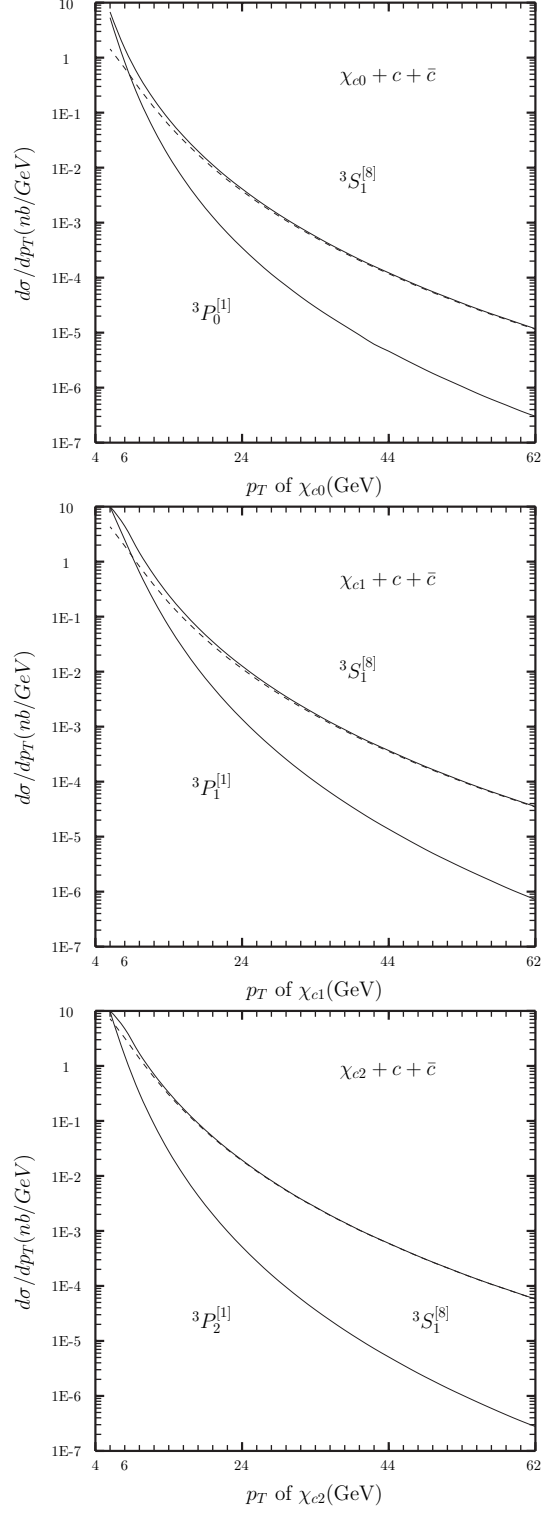


FIG. 7: Differential cross sections of $\chi_{cJ} + c + \bar{c}$ as functions of transverse momentum at the LHC with $\sqrt{s} = 7$ TeV and rapidity cut $2 < y_{\chi_{cJ}} < 4.5$. The dashed line denotes CO contribution, and the solid line denotes CS contribution.

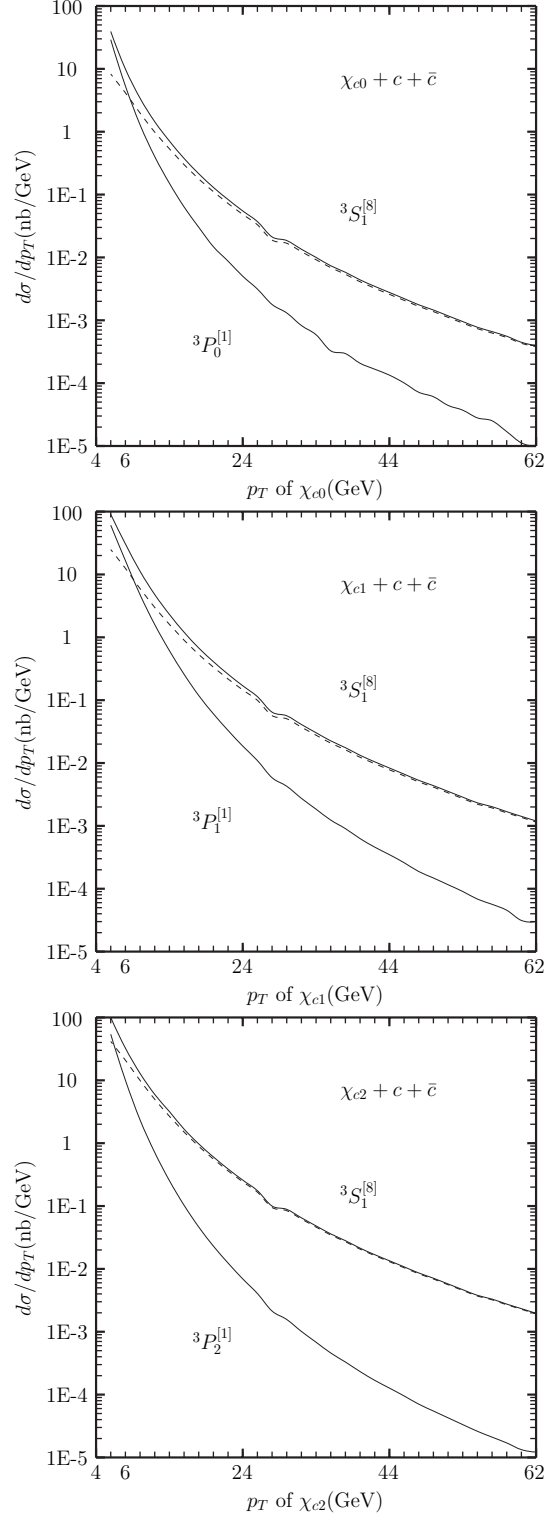


FIG. 8: Differential cross sections of $\chi_{cJ} + c + \bar{c}$ as functions of transverse momentum at the LHC with $\sqrt{s} = 14\text{TeV}$ and rapidity cut $|y_{\chi_{cJ}}| < 3.0$. The dashed line denotes CO contribution, and the solid line denotes CS contribution.

change the results obtained in this work. Another notable result in this work is that the CO contribution dominates over $\chi_{cJ} + c + \bar{c}$ production at large p_T (say, $p_T > 7\text{GeV}$), therefore measuring the process at hadron colliders, especially at the LHC, may provide important information for the production mechanism of heavy quarkonium, while the experiment itself may also be very interesting and challenging in view of the complexity of the measurement.

Acknowledgement

We thank Rong Li for valuable help in Fortran program of phase space integration and Yu-Jie Zhang and Kai Wang and Ce Meng for helpful discussions. This work was supported by the National Natural Science Foundation of China (No.11021092, No.11075002) and the Ministry of Science and Technology of China (No.2009CB825200).

Appendix

We list all the fermion chains encountered in our calculation as follows.

$$f_0(q_1, q_2, \lambda_1, \lambda_2) = \langle q_{0\lambda_1} | (\not{q}_1 + m) \gamma_\delta (\not{q}_2 - m) | q_{0\lambda_2} \rangle, \quad (21)$$

$$f_1(q_1, q_2, k, \lambda_1, \lambda_2, \lambda_3) = \langle q_{0\lambda_1} | (\not{q}_1 + m) \gamma_\delta (\not{k} - \not{q}_2 + m) \not{\epsilon}^{\lambda_3}(k, q_0) (\not{q}_2 - m) | q_{0\lambda_2} \rangle, \quad (22)$$

$$f_2(q_1, q_2, k, \lambda_1, \lambda_2, \lambda_3) = \langle q_{0\lambda_1} | (\not{q}_1 + m) \not{\epsilon}^{\lambda_3}(k, q_0) (\not{q}_1 - \not{k} + m) \gamma_\delta (\not{q}_2 - m) | q_{0\lambda_2} \rangle, \quad (23)$$

$$f_3(q_1, q_2, k, \lambda_1, \lambda_2, \lambda_3) = \langle q_{0\lambda_1} | (\not{q}_1 + m) \not{\epsilon}^{\lambda_3}(\not{q}_2 - m) | q_{0\lambda_2} \rangle, \quad (24)$$

$$f_4(q_1, q_2, k_1, k_2, \lambda_1, \lambda_2, \lambda_3, \lambda_4) = \langle q_{0\lambda_1} | (\not{q}_1 + m) \gamma_\delta (\not{k}_1 + \not{k}_2 - \not{q}_2 + m) \not{\epsilon}^{\lambda_3}(k_1, q_0) (\not{k}_2 - \not{q}_2 + m) \not{\epsilon}^{\lambda_4}(k_2, q_0) (\not{q}_2 - m) | q_{0\lambda_2} \rangle, \quad (25)$$

$$f_5(q_1, q_2, k_1, k_2, \lambda_1, \lambda_2, \lambda_3, \lambda_4) = \langle q_{0\lambda_1} | (\not{q}_1 + m) \not{\epsilon}^{\lambda_3}(k_1, q_0) (\not{q}_1 - \not{k}_1 + m) \gamma_\delta (\not{k}_2 - \not{q}_2 + m) \not{\epsilon}^{\lambda_4}(k_2, q_0) (\not{q}_2 - m) | q_{0\lambda_2} \rangle, \quad (26)$$

$$f_6(q_1, q_2, k_1, k_2, \lambda_1, \lambda_2, \lambda_3, \lambda_4) = \langle q_{0\lambda_1} | (\not{q}_1 + m) \not{\epsilon}^{\lambda_3}(k_1, q_0) (\not{q}_1 - \not{k}_1 + m) \not{\epsilon}^{\lambda_4}(k_2, q_0) (\not{q}_1 - \not{k}_1 - \not{k}_2 - m) \gamma_\delta (\not{q}_2 - m) | q_{0\lambda_2} \rangle, \quad (27)$$

$$f_7(q_1, q_2, k_1, k_2, \lambda_1, \lambda_2, \lambda_3, \lambda_4) = \langle q_{0\lambda_1} | (\not{q}_1 + m) \not{\epsilon}^{\lambda_3}(k_1, q_0) \not{\epsilon}^{\lambda_4}(k_2, q_0) \gamma_\delta (\not{q}_2 - m) | q_{0\lambda_2} \rangle, \quad (28)$$

$$f_8(q_1, q_2, k_1, k_2, \lambda_1, \lambda_2, \lambda_3, \lambda_4) = \langle q_{0\lambda_1} | (\not{q}_1 + m) \gamma_\delta \not{\epsilon}^{\lambda_3}(k_1, q_0) \not{\epsilon}^{\lambda_4}(k_2, q_0) (\not{q}_2 - m) | q_{0\lambda_2} \rangle, \quad (29)$$

$$f_9(q_1, q_2, k_1, k_2, \lambda_1, \lambda_2, \lambda_3, \lambda_4) = \langle q_{0\lambda_1} | (\not{q}_1 + m) \not{\epsilon}^{\lambda_3}(k_1, q_0) (\not{q}_2 - m) | q_{0\lambda_2} \rangle, \quad (30)$$

where $q_1^2 = q_2^2 = m_c^2$, k, k_1, k_2 and q_0 are light-like vectors.

-
- [1] K.Abe *et al.*[BELLE Collaboration], Phys. Rev. Lett. **89**, 142001 (2002) [arXiv:hep-ex/0205104].
 - [2] P. Pakhlov *et al.*[BELLE Collaboration], Phys. Rev. **D79**, 071101 (2009) [arXiv:0901.2775[hep-ex]].
 - [3] Yu-Jie Zhang, Kuang-Ta Chao, Phys. Rev. Lett. **98**, 092003 (2007) [arXiv: hep-ph/0611086]; Bin Gong, Jian-Xiong Wang, Phys. Rev. **D80**, 054015 (2009) [arXiv: 0904.1103[hep-ph]].
 - [4] Yan-Qing Ma, Yu-Jie Zhang and Kuang-Ta Chao, Phys. Rev. Lett.**102**, 162002 (2009)[arXiv:0812.5106[hep-ph]]; Bin Gong, Jian-Xiong Wang, Phys. Rev. Lett. **102**, 162003 (2009) [arXiv:0901.0117[hep-ph]].
 - [5] Yu-Jie Zhang, Yan-Qing Ma, Kai Wang and Kuang-Ta Chao, Phys. Rev. **D81**, 034015 (2010) [arXiv: 0911.2166[hep-ph]].
 - [6] Rong Li and Jian-Xiong Wang, Phys. Rev. D **82**, 054006 (2010) [arXiv:1007.2368 [hep-ph]].
 - [7] P. Abreu *et al.* [DELPHI Collaboration], Phys. Lett. **B341**, 109 (1994); M. Wadhwa *et al.* [L3 Collaboration], Nucl. Phys. Proc. Suppl. **64**, 441 (1998); G. Alexander *et al.* [OPAL Collaboration], Phys. Lett. **B384**, 343 (1996); M. Acciarri *et al.* [L3 Collaboration], Phys. Lett. **B453**, 94 (1999).
 - [8] Rong Li and Kuang-Ta Chao, Phys. Rev. D **79**, 114020 (2009) [arXiv: 0904.1643[hep-ph]].
 - [9] J. Abdallah *et al.* [DELPHI Collaboration], Phys. Lett. **B565**, 76 (2003) [arXiv: hep-ex/0307049].
 - [10] P. Artoisenet, J.P. Lansberg and F. Maltoni, Phys. Lett. **B653**, 60-66 (2007)[arXiv:hep-ph/0703129].
 - [11] Zhi-Guo He, Rong Li and Jian-Xiong Wang, Phys. Rev. **D79**, 094003 (2009) [arXiv:0904.2069[hep-ph]].
 - [12] J. M. Campbell, F. Maltoni and F. Tramontano, Phys. Rev. Lett. **98**, 252002 (2007) [arXiv:hep-ph/0703113]; Bin Gong, Jian-Xiong Wang, Phys. Rev. Lett. **100**, 232001 (2008) [arXiv: 0802.3727[hep-ph]]; Bin Gong, Jian-Xiong Wang, Phys. Rev. **D78**, 074011 (2008) [arXiv: 0805.2469[hep-ph]]; Rong Li, Jian-Xiong Wang, Phys. Lett. **B672**, 51-55 (2009) [arXiv:0811.0963[hep-ph]].

- [13] F. Abe *et al.* [CDF Collaboration], Phys. Rev. Lett. **79**, 572, 578 (1997); A. A. Affolder *et al.* [CDF Collaboration], Phys. Rev. Lett. **85**, 2886 (2000)[arXiv:hep-ex/0004027].
- [14] Zhi-Guo He, Jian-Xiong Wang, Phys. Rev. **D81**, 054030 (2010) [arXiv:0911.0139[hep-ph]].
- [15] G. T. Bodwin, E. Braaten and G. P. Lepage, Phys. Rev. **D51**, 1125 (1995) [Erratum-ibid. **D55**, 5853 (1997)] [arXiv:hep-ph/9407339].
- [16] A. Abulencia *et al.* [CDF Collaboration], Phys. Rev. Lett. **98**, 232001 (2007) [arXiv: hep-ex/0703028].
- [17] Yan-Qing Ma, Kai Wang and Kuang-Ta Chao, Phys. Rev. **D83**, 111503(R) (2011)[arXiv: 1002.3987[hep-ph]].
- [18] T. Hahn, Comput. Phys. Commun. **140**, 418 (2001).
- [19] Chao-Hsi Chang, Chafik Driouichi, Paula Eerola, Xing-Gang Wu, Comput. Phys. Commun. **159**, 192-224 (2004) [arXiv:hep-ph/0309120].
- [20] D.Maitre and P.Mastrolia, Comput. Phys. Commun. **179**, 501-574 (2008)[arXiv: 0710.5559[hep-ph]].
- [21] Dan Li, Zhi-Guo He and Kuang-Ta Chao, Phys. Rev. **D80**, 114014 (2009) [arXiv: 0910.4155[hep-ph]].
- [22] Chao-Hsi Chang, Jian-Xiong Wang, Xing-Gang Wu, Phys.Rev. **D70**, 114019 (2004) [arXiv:hep-ph/0409280].
- [23] G. P. Lepage, “Vegas: An Adaptive Multidimensional Integration Program”.
- [24] E.J. Eichten and C. Quigg, Phys. Rev. **D52**, 1726 (1995).
- [25] B. A. Kniehl, G. Kramer and C. P. Palisoc, Phys. Rev. **D68**, 114002 (2003) [arXiv: hep-ph/0307386]; B. A. Kniehl and J. Lee, Phys. Rev. **D62**, 114027 (2000).
- [26] K. Nakamura *et al.* [Particle Data Group], J. Phys. G **37**, 075021 (2010).
- [27] Yan-Qing Ma, Kai Wang, Kuang-Ta Chao, Phys. Rev. Lett. **106**, 042002 (2011) [arXiv: 1009.3655[hep-ph]].